

Non-equilibrium Pair Breaking in $\text{Ba}(\text{Fe}_{1-x}\text{Co}_x)_2\text{As}_2$ Superconductors: Evidence for Formation of Photo-Induced Excitonic Spin-Density-Wave State

X. Yang¹, L. Luo¹, M. Mootz², A. Patz¹, S. L. Bud'ko¹, P. C. Canfield¹, I. E. Perakis², and J. Wang¹

¹*Department of Physics and Astronomy and Ames Laboratory-U.S. DOE,
Iowa State University, Ames, Iowa 50011, USA.*

²*Department of Physics, University of Alabama at Birmingham, Birmingham, AL 35294-1170, USA.*
(Dated: March 9, 2024)

Ultrafast terahertz (THz) pump-probe spectroscopy reveals unusual out-of-equilibrium Cooper pair dynamics driven by femtosecond (fs) optical quench of superconductivity (SC) in iron pnictides. We observe a two-step quench of the SC gap, where an abnormally slow (many 100's of ps) quench process is clearly distinguished from the usual fast (sub-ps) hot-phonon-mediated scattering channel. This pair breaking dynamics depends strongly on doping, pump fluence, and temperature. The above observations, together with quantum kinetic modeling of non-equilibrium SC and magnetic correlations, provide evidence for photogeneration of a transient state where SC competes with build-up of spin-density-wave (SDW) excitonic correlation between quasi-particles (QP).

PACS numbers: 74.25.Gz, 74.20.-z, 78.47.J-, 74.70.Xa, 74.40.Gh

Ultrafast optical tailoring of transient quantum states provides a new way to discover, design, and control exotic correlated materials phases. Recent examples include, among others, quantum femtosecond magnetism [1] and laser-induced superconductivity [2]. This strategic approach is implemented by non-thermal separation, within a certain time window, of distinct coupled orders. The latter are strongly intertwined in equilibrium, but respond differently to strong fs photoexcitation [3, 4]. Iron-arsenide based superconductors (FeSCs) [5] are well-suited for such non-equilibrium control, as their properties are determined by competing SC, SDW, nematic and structural orders [6]. Here we address two open issues in FeSCs: (i) how to use non-equilibrium SC pairing/pair breaking to distinguish between two different bosonic channels, i.e., phonon and SDW, that determine the SC and excitation properties, (ii) how instabilities in two different correlation channels, i.e., Cooper and excitonic, can lead to controllable transient states.

Ultrafast THz spectroscopy is well-suited for disentangling strongly-coupled excitations. In SCs, this can be achieved by directly probing out-of-equilibrium Cooper pairs and their dynamics following strong pump photoexcitation. By tuning the THz probe frequency in the vicinity of the SC gaps $2\Delta_{SC}$ of few meV, low-frequency THz electrodynamics can be used to directly measure the time evolution of a SC condensate. The latter is “suddenly” driven away from equilibrium, by fs optical excitation here, as illustrated in Fig. 1(a). Previous pump-probe experiments showed that the dynamic evolution of a SC condensate following high-frequency optical pump mostly comes from its interactions with hot bosonic excitations [7, 8]. In FeSCs, both phonon and SDW channels with distinct ultrafast responses are expected to play an important role. Although the SC dynamics in FeSCs has been measured before in the optical high frequency region [9], time-resolved THz spectroscopy experiments in

the SC states have been scarce so far.

Photogeneration of non-equilibrium states in quantum materials with competing SC and density wave orders, such as the FeSCs, provides an opportunity to elucidate the role of electron-hole (e - h) channels, in addition to Cooper channel, in high- T_c superconductivity. In equilibrium, the SDW phase of FeSCs shows a spontaneous coherence emerging from nested e -like and h -like Fermi sea pockets, with transition to a $(0, \pi)/(\pi, 0)$ spin-stripped state [10, 11]. Following photoexcitation of QPs in the e and h pockets, an excitonic instability can be triggered by the residual inter-pocket magnetic interaction (illustrated in Fig. 1(b)). We refer to a QP e - h pair state as an excitonic SDW state. Such out-of-equilibrium collective behavior remains, however, elusive so far.

In this letter, we present an ultrafast THz spectroscopy investigation of the non-equilibrium dynamics of the SC order in $\text{Ba}(\text{Fe}_{1-x}\text{Co}_x)_2\text{As}_2$. We find that Cooper pair breaking subsequent to strong fs optical excitation follows an unusual two-step temporal profile. In particular, the usual phonon scattering channel (τ_{Fast}) is distinguished from an additional very slow SC quench (τ_{Slow}). The latter lasts for many 100's of ps under strong pumping. The pump fluence dependence of the SC quench differs significantly between the under- and overdoped regimes with different SDW coherence. The remarkably slow pair-breaking dynamics, together with quantum kinetic modeling, provide evidence for the formation of a non-equilibrium correlated state of QP e - h pairs competing with SC, which is driven by excitonic correlation of the disconnected Fermi sea pockets.

The samples are single-crystalline $\text{Ba}(\text{Fe}_{1-x}\text{Co}_x)_2\text{As}_2$ with cobalt substitutions of $x=0.047$ and 0.1. In the underdoped sample ($x=0.047$), long-range SDW and structural phase transitions appear at $T_N=48$ K and $T_S=66$ K, respectively [11]. The phase transitions are *absent* in the overdoped sample ($x=0.100$). Both samples

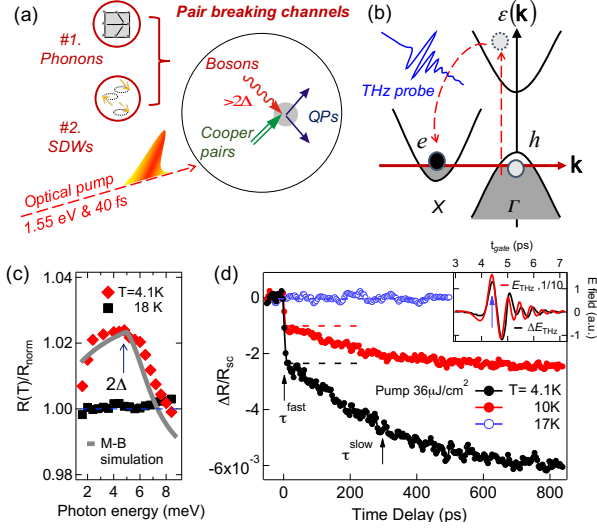


Figure 1. Schematics of SC pair breaking channels, (a), and interband transitions, (b), after fs pump photoexcitation. (c): Static THz reflectivity spectra, normalized to the normal state spectra at 20 K, for underdoped $x = 0.047$ sample, at 4.1 K and 18 K. Grey line shows the result of the Mattis-Bardeen theory. (d) Ultrafast THz dynamics for the above underdoped sample. Inset: The measured time-dependent THz field transients, with gate-time (blue arrow) $t_{\text{gate}} = 4.4$ ps, at $T = 4.1$ K.

exhibit a SC transition at $T_C \sim 17$ K. Our optical pump–THz probe reflectivity spectroscopy setup is described in detail elsewhere [12]. The opaque sample is mounted at 45° to incident light and cooled to $T = 4.1$ K.

We start with the equilibrium THz measurements of the static SC order and energy gap. The typical static THz reflection spectra, $R(T)$, of $\text{Ba}(\text{Fe}_{0.953}\text{Co}_{0.047})_2\text{As}_2$ are shown in Fig. 1(c). We compare temperatures $T = 4.1$ K (red diamonds) and 18 K (black rectangles), below and above the SC transition respectively. These spectra are obtained through Fourier transform of the measured time domain THz field traces, e.g., the red-line curve in the inset of Fig. 1(d). They are normalized by the normal state 20 K trace (not shown). The ratio $R(4.1\text{ K})/R(20\text{ K})$ in the measured spectral range of 1–11 meV exhibits the characteristic SC profile. The distinct upward cusp with maximum at ~ 5 meV reflects the SC energy gap $2\Delta_{\text{SC}}$. In contrast, $R(18\text{ K})/R(20\text{ K}) \sim 1$ has a featureless spectral shape. The measured reflectivity spectra are reproduced well by the Mattis-Bardeen (MB) theory and by Fresnel equations. In the low-frequency/temperature limit, the measured ratio can be expressed as $1 + 4\sqrt{\omega/(\pi\sigma_{1N})}$, where σ_{1N} is the normal state conductivity.

The ultrafast THz differential reflectivity $\Delta R/R_{\text{SC}}$ in the underdoped compound is shown in Fig. 1(d) for three different temperatures, 4.1 K, 10 K and 17 K. The pump fluence and photon energy are set to $40\text{ }\mu\text{J}/\text{cm}^2$ and

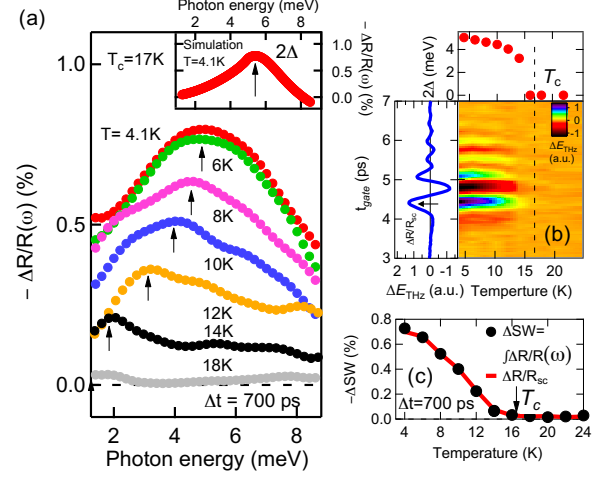


Figure 2. (a) THz differential reflectivity spectra (dots) for the $x = 0.047$ sample at 700 ps. The cusp peak marked by black arrows reflects $2\Delta_{\text{SC}}$. Inset shows the MB simulation (see text). (b) Temperature-dependent $\Delta E/E$ THz transients. Left panel: $\Delta E/E$ transient at 4.1 K. Top panel: temperature dependence of $2\Delta_{\text{SC}}$. (d) Temperature dependence of the integrated spectral weight and peak transient amplitude.

1.55 eV, respectively. The transient signals are given by the difference of the time-dependent THz fields in the photo-excited (pump on, back line, inset) and un-excited (pump off) states (red line, inset). $\Delta R/R_{\text{SC}}$ is then obtained as $[(E_{\text{THz}} + \Delta E_{\text{THz}})^2 - E_{\text{THz}}^2]/E_{\text{THz}}^2$. The $\Delta R/R_{\text{SC}}$ dynamics at a fixed gate time $t_{\text{gate}} = 4.4$ ps (blue arrow, inset) is recorded as function of pump–probe delay. Fig. 1(d) demonstrates a distinct two-step temporal profile of pair-breaking dynamics. The initial sub-ps SC gap decrease (τ_{Fast}) is followed by a further very slow SC quench that lasts for an unusually long time ~ 800 ps (τ_{Slow}). The strong temperature dependence in Fig. 1(d) coincides with the SC transition. Approaching the critical temperature from below, the transient signals quickly decrease, as seen in the 4.1 K (black circle) and 10 K traces (red), and diminish at $T \approx T_C \approx 17$ K (blue).

We now present transient $\Delta R(\omega)/R_{\text{SC}}$ spectra that further point to non-equilibrium pair-breaking as the origin of the pump-induced THz signals. Figure 2(a) shows the temperature-dependent low frequency, ~ 1 – 9 meV, differential reflectivity spectra of the underdoped $x = 0.047$ sample at a fixed long time delay of 700 ps. These spectra are obtained from the Fourier transform of the time-domain THz raw data (Fig. 2(b)). We note three distinct features of $\Delta R(\omega)/R_{\text{SC}}$: (1) The negative low frequency change $\Delta R(\omega)/R_{\text{SC}} < 0$ indicates photo-induced condensate breaking processes. (2) The pump-probe transient spectra exhibit the characteristic SC line-

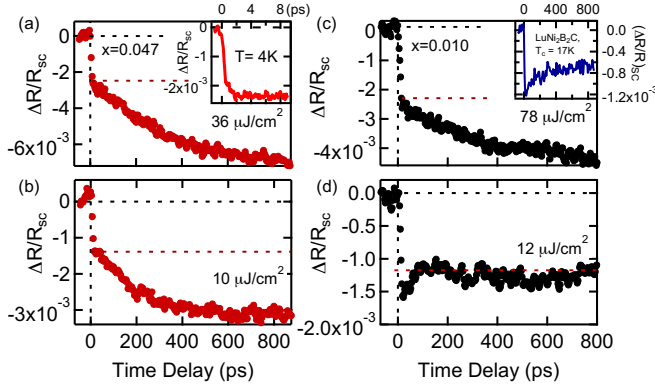


Figure 3. Ultrafast THz pump probe scan at different pump fluences for (a,b) $x=0.047$ and (c,d) $x=0.1$ samples. All traces taken in the superconducting state at $T=4.1$ K. Inset of (a): the initial dynamics. Inset of (c): The THz dynamics in $\text{LuNi}_2\text{B}_2\text{C}$ at pump fluence of $40 \mu\text{J}/\text{cm}^2$.

shape with cusp peak at $2\Delta_{\text{SC}}$ (black arrow). This line-shape can be reproduced well by the MB theory, as shown in the inset of Fig. 2(a). (3) Approaching the critical temperature from below, we see that $\Delta R(\omega)/R_{\text{SC}}$ quickly diminish as the cusp at $2\Delta_{\text{SC}}$ shifts to lower frequencies (black arrows, Fig. 2(a)). This SC gap temperature dependence is summarized in the top panel of Fig. 2(b). In addition, we compared the integrated reflectivity spectral weight associated with the SC states and the $\Delta R/R_{\text{SC}}$ amplitude at $t_{\text{gate}}=4.4$ ps. The strong correlation between the two at all temperatures (Fig. 2(c)) and fluences (inset, Fig. 4(b)), allows us to study the ultrafast pair-breaking dynamics by recording $\Delta R/R_{\text{SC}}$ as in Fig. 1(d).

Next we show the strong dependence of the non-equilibrium SC quench profile on pump fluence and doping. Figs. 3(a) and 3(b) show the photoinduced $\Delta R/R_{\text{SC}}$ dynamics in the underdoped, $x=0.047$, sample and compare $36 \mu\text{J}/\text{cm}^2$ and $10 \mu\text{J}/\text{cm}^2$ pumping. Both excitations of the coupled SC/SDW ground state order show a sub-ps τ_{Fast} followed by a 100's ps τ_{Slow} process. Previous works in BCS and cuprate SCs have shown that the majority of the absorbed photon energy transfers to the phonon reservoir during the pulse [8]. Hot phonons then deplete the condensate on a few-ps timescale [7, 16]. This time interval becomes shorter (sub-ps) under the strong pumping used here, consistent with the inset of Fig. 3(a). Here the slow ~ 800 ps SC quench under strong pumping appears to be different from other superconductors (supplementary). For comparison, the inset of Fig. 3(c) shows the non-equilibrium pair breaking dynamics of the BCS superconductor $\text{LuNi}_2\text{B}_2\text{C}$. Unlike for the FeSCs, similar strong pumping of this superconductor exhibits single-step, sub-ps SC quenching, followed by

partial recovery and long decay. This typical pair breaking temporal profile is consistent with the τ_{Fast} component in the FeSCs. It can be explained in terms of QP scattering with high energy phonons, followed by condensate recovery governed by phonon relaxation [7]. A comparison of the two SC systems indicates that the additional, remarkably slow and yet strong, channel is exclusively present in the FeSCs. This appears to be distinct from the usual hot phonon bosonic channel. The continuing SC gap quench over many 100s of ps is “intrinsic” and unlikely to come from, e.g., heat diffusion, which would appear in both studied systems.

Figs. 3(c) and (d) show our results in the overdoped FeSC system ($x=0.1$), where there is no long-range SDW order in equilibrium. In this regime of the phase diagram, the quench temporal profile changes drastically with increasing pump fluence different from the underdoped regime. For example, while the slow SC quench is again seen at high fluences $78 \mu\text{J}/\text{cm}^2$ (Fig. 3(c)), at low pump fluences ($12 \mu\text{J}/\text{cm}^2$ in Fig. 3(d)) the initial fast quench is followed by a partial recovery similar to the BCS sample (inset, Fig. 3(c)). Our results show that, for the overdoped ground state without SDW coherence, the slow SC quench channel only appears above a critical fluence. While in the underdoped regime with SC/SDW ground state, it persists down to much lower fluences. Such a strong distinction between sample doping corroborates that the continuing SC gap quench is “intrinsic” in FeSCs that differs from both BCS and cuprate SCs.

The striking fluence and doping dependences of the FeSC condensate quench are seen more clearly in Figs. 4(a) and 4(b). Here, the integrated spectral weight (SW), obtained from the peak-peak amplitude change $\Delta R/R_{\text{SC}}$ at $t_{\text{gate}}=4.4$ ps (inset, Fig. 4(b)), is shown as function of pump fluence and compared between underdoped and overdoped regimes. Fig. 4(a) compares the fluence dependence in the overdoped regime (no SDW ground state coherence) between short 5 ps (red empty circle) and long 700 ps (black solid circle) time delays. The SC quench as function of photocarrier density is qualitatively different at short and long times and the two curves cross at $\sim 25 \mu\text{J}/\text{cm}^2$. In particular, at $\Delta t=700$ ps, we observe a transition from SC to normal state above a large critical pump fluence, $I_q=182 \mu\text{J}/\text{cm}^2$. Such transition is not observed at 5ps in the measured range, where the signal appears to saturate for high fluences. Fig. 4(b) compares this SC-to-normal state transition at $\Delta t=700$ ps between the under- and overdoped samples. In the underdoped regime with SC/SDW coherence ($x=0.047$), the transition occurs at much smaller critical pump fluence $\sim 50 \mu\text{J}/\text{cm}^2$ than in the overdoped regime without SDW coherence. Below we provide an interpretation of these salient experimental features based on quantum kinetic calculations of photoinduced build-up of SDW excitonic correlation between the photoexcited e and h QPs.

The conventional Rotwarth-Taylor (RT) model [7, 17],

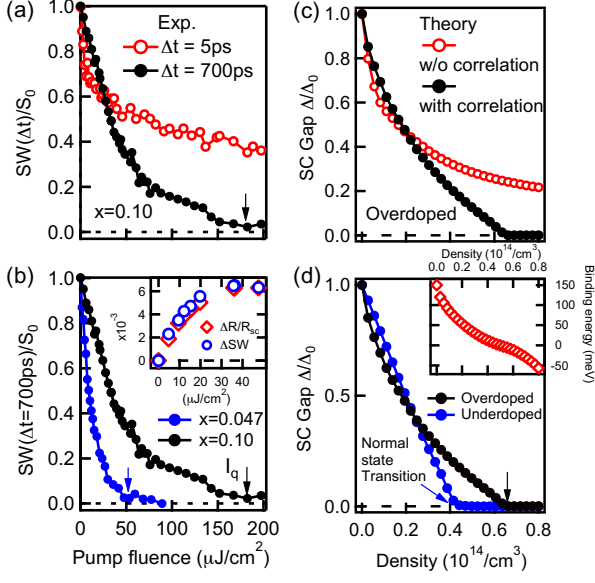


Figure 4. Measured fluence dependence of the integrated spectral weight (SW): (a) $x=0.1$ crystal at 5 ps (red) and 700 ps (black); (b) comparison of $x=0.047$ and $x=0.1$ samples at 700 ps. Inset: SW and $\Delta R/R_{SC}$ exhibit the same fluence dependence. (c) Theoretical modeling of the SC gap quench in the overdoped region as function of photoexcited QP density ρ , with (black line) or without (red line) inter-pocket excitonic correlation. The y -axis is normalized by the equilibrium SC gap Δ_0 . (d) Theoretical comparison of under- and over-doped regions for the photoinduced correlated SDW excitonic state. Inset: Excitonic energy $|E|$, Eq. (1), as function of ρ .

which describes QP interactions with a hot boson bath whose properties are not strongly affected by photoexcitation, does not provide a consistent fit of our experimental data (supplementary). There we summarize a density matrix equation-of-motion calculation of the QP population dynamics arising from the strong inter-pocket magnetic interaction in FeSCs. We focus on the build-up of e - h excitonic correlation after initial photocarrier relaxation [4]. The latter results in hot QP populations of disconnected e - and h -like Fermi sea pockets (Fig. 1(b)). Subsequently, interband residual interactions between such QPs can form excitonic pairs prior to inter-pocket relaxation that requires a large momentum transfer (Fig. 1(b)). Slow ps formation of Coulomb-bound excitonic correlation prior to interband recombination has been previously established in semiconductors [18].

Our starting point for describing the QP population dynamics is the model of Refs. [14, 15]. This model captures the most essential features of the competition between SC and SDW orders in the FeSCs. Assuming for simplicity one e and one h pocket, we first transform to the basis of Bogoliubov quasi-particles with both SC

and SDW coherence. We then study the effects of the residual inter-pocket interaction among these QPs in the SDW channel. High frequency pump excitation and fast photocarrier scattering with phonons creates QP incoherent distributions in both e and h pockets within 100fs timescales [4]. These hot distributions create an initial condition for subsequent non-thermal time evolution of QP e and h populations $n_{\mathbf{p}}$ coupled by inter-pocket e - h correlation. The latter is driven by the residual QP inter-band interaction, which leads to Coulomb-correlated QP pairs (spin excitons) with total momentum determined by the difference between the e and h pockets. For our purposes here, we consider quasi-stationary solutions of the equations of motion. Prior to inter-pocket relaxation, we thus obtain a correlated SDW state formed by QP e - h pairs with amplitude $\phi_{\mathbf{p}}$. The latter is described by the generalized Wannier equation (supplementary)

$$(\varepsilon_{\mathbf{p}}^- + \varepsilon_{\mathbf{p}}^+) \phi_{\mathbf{p}} - (1 - 2n_{\mathbf{p}}) \sum_{\mathbf{k}} V_{\mathbf{k},\mathbf{p}} \phi_{\mathbf{k}} = E \phi_{\mathbf{p}}. \quad (1)$$

Here, $\varepsilon_{\mathbf{p}}^-$ and $\varepsilon_{\mathbf{p}}^+$ are the single-QP energies and $V_{\mathbf{k},\mathbf{p}}$ are the interband Coulomb matrix elements describing the residual interaction. The energy eigenvalue E describes excitonic corrections to the chemical potential, which develop as correlation builds up between the photoexcited QPs. E depends on the total photoexcited QP density ρ through the condition $\rho = \sum_{\mathbf{p}} n_{\mathbf{p}}$, where the QP distribution $n_{\mathbf{p}}$ is determined by (supplementary)

$$\left(n_{\mathbf{p}} - \frac{1}{2}\right)^2 + |\phi_{\mathbf{p}}|^2 = \frac{1}{4}. \quad (2)$$

The above equations, together with SC/SDW order parameter equations discussed in the supplement, provide a self-consistent calculation of a correlated SDW/SC photoexcited state prior to inter-pocket recombination. They are similar to the description of incoherent excitonic correlation build-up in semiconductors [18] and transition between Bose condensation and BCS superconductivity in the case of fermions with attractive interaction [19]. Here we describe QP e - h pair states whose properties depend on the SC and SDW coherence analogous to Ref. [13]. This introduces a doping dependence that depends on the Fermi sea topology. Eq. (1) interpolates between the weak and strong coupling limits and can have both bound and unbound solutions, depending on QP density ρ , Pauli blocking effects, and inter-pocket interaction strength. With increasing ρ , the momentum dependence and magnitude of the QP distribution $n_{\mathbf{p}}$ changes strongly due to its coupling with the QP pair amplitude $\phi_{\mathbf{p}}$. This, in turn, affects the Pauli blocking effects that quench the SC gap.

Fig. 4(c) compares the calculated quasi-stationary SC gap with or without the excitonic correlation $\phi_{\mathbf{p}}$ as a function of total QP density ρ . Since the pump-induced photocarriers have already relaxed during the initial ps

quench, we model the initial condition by assuming quasi-equilibrium Fermi–Dirac QP distributions with hot temperature determined by the total ρ (supplementary material). Fig. 4(c) shows the effects of SDW exciton formation on the SC gap in the overdoped regime, where only SC order is present in the ground state. The calculated SC gap without excitonic QP correlation, $\phi_p=0$ (red circles), shows a fast decrease at low QP densities, which flattens (saturates) as ρ increases further. This feature is in qualitative agreement with the measured fluence dependence of the SC gap at short ps time delays (red circles, Fig. 4(a)). During short timescales, excitonic correlation has not had time to built-up yet and thus $\phi_p \approx 0$. The Pauli blocking saturation behavior of the SC gap with increasing ρ results from the momentum dependence of n_p , which for $\phi_p=0$ is similar to the simple BCS theory [20].

With $\phi_p \neq 0$ at later times, the QP distribution n_p changes drastically. Our calculations show that SDW excitonic formation leads to a complete quench of the SC gap at elevated ρ (black curve in Fig. 4(c)). The complex photoinduced interplay of an emergent correlated SDW state with the SC condensate thus results in a transition from SC to normal state above a critical pump fluence. This result is in qualitative agreement with the measured fluence dependence of the SC gap at 700 ps (black circles, Fig. 4(a)). It supports our claim that the experimentally observed qualitative difference in the SC gap fluence dependence between long and short times arises from the delayed formation of a correlated SDW state. The latter requires build-up of excitonic correlation between the laser-induced e and h QP populations.

Figure 4(d) compares the calculated QP density dependence of the SC gap at long times between the underdoped (blue solid circle) and overdoped (black solid circle) regimes. The doping dependence of the critical pump fluence required for SC-to-normal state transition is in qualitative agreement with the experiment (compare to Fig. 4(b)). While in the overdoped regime SC order can only compete with photoinduced SDW excitonic order, the additional condensed SDW coherence present in the underdoped regime results in SC-to-normal state transition at lower photoexcited QP densities. Such doping dependence of the residual e - h correlations comes from the differences in coherence and Fermi sea pockets between the overdoped and underdoped regimes. Finally, the inset of Figure 4(d) shows the calculated energy eigenvalue E per e - h pair as a function of QP density ρ . At low ρ , we obtain a bound SDW excitonic state, which however becomes unbound due to phase-space filling Pauli effects.

In conclusion, we performed the first ultrafast THz spectroscopy in FeSCs to demonstrate the existence of an additional, remarkably slow, pair-breaking channel. This is consistent with our theoretical prediction that the build-up of SDW excitonic correlation between laser-induced e and h QPs manifests itself in the long-time

THz formation dynamics with strong pump-fluence and doping dependence. The fast control demonstrated here by adjusting both pump fluence and doping may be used to access hidden density-wave phases and quantum criticality under the SC dome in high- T_c superconductors.

ACKNOWLEDGEMENT

This work was supported by the Army Research office under award W911NF-15-1-0135 (THz spectroscopy). Theory work at the University of Alabama, Birmingham was supported by start-up funds. Sample growth, characterization and phase diagram analysis (PCC and SLB) was supported by the Ames Laboratory, the US Department of Energy, Office of Science, Basic Energy Sciences, Materials Science and Engineering Division under contract #DE-AC02-07CH11358. THz instrument was supported in part by the Keck Foundation (J.W.).

-
- [1] T. Li, A. Patz, L. Mouchliadis, J. Yan, T. A. Lograsso, I. E. Perakis, and J. Wang, *Nature* **496**, 69 (2013); P. C. Lingos, A. Patz, T. Li, G. D. Barmparis, A. Keliri, M. D. Kapetanakis, L. Li, J. Yan, J. Wang, and I. E. Perakis, *Phys. Rev. B* **95**, 224432 (2017).
 - [2] D. Fausti, R. I. Tobey, N. Dean, S. Kaiser, A. Dienst, M. C. Hoffmann, S. Pyon, T. Takayama, H. Takagi, and A. Cavalleri, *Science* **331**, 14 (2011); for a review see R. Mankowsky, M. Fechner, M. Frst, A. von Hoegen, J. Porras, T. Loew, G. L. Dakovski, M. Seaberg, S. Möller, G. Coslovich, B. Keimer, S. S. Dhesi, and A. Cavalleri, *Structural Dynamics* **4**, 044007 (2017).
 - [3] A. Patz, et al., *Nat. Commun.* **5**, 3229 (2014); A. Patz, et al., *Phys. Rev. B* **95**, 165122 (2017).
 - [4] M. Porer, U. Leierseder, J.-M. Menard, H. Dachraoui, L. Mouchliadis, I. E. Perakis, U. Heinzmann, J. Demsar, K. Rossnagel, and R. Huber *Nat. Mater.* **13**, 857 (2014)
 - [5] Y. Kamihara, T. Watanabe, M. Hirano, and H. Hosono, *J. Am. Chem. Soc.* **130**, 3296 (2008).
 - [6] P. C. Canfield and S. L. Bud, *Annu. Rev. Condens. Phys* **1**, 27 (2010).
 - [7] V. V. Kabanov, J. Demsar, and D. Mihailovic, *Phys. Rev. Lett.* **95**, 147002 (2005).
 - [8] For review, see, e.g., C. Giannetti, M. Capone, D. Fausti, M. Fabrizio, F. Parmigiani, and D. Mihailovic, *Advances in Physics* **65**, 58 (2016).
 - [9] Mertelj, T., *et.al.*, *Phys. Rev. Lett.*, **102**, 117002 (2009); Chia, E. E. M. *et.al.*, *Phys. Rev. Lett.*, **104**, 027003 (2010); Torchinsky, *et.al.*, *Phys. Rev. Lett.*, **105**, 027005 (2010).
 - [10] N. Ni, M. E. Tillman, J.-Q. Yan, A. Kracher, S. T. Hannahs, S. L. Bud'ko, and P. C. Canfield, *Phys. Rev. B* **78**, 214515 (2008).
 - [11] S. Nandi, M. G. Kim, A. Kreyssig, R. M. Fernandes, D. K. Pratt, A. Thaler, N. Ni, S. L. Bud, P. C. Canfield, J. Schmalian, R. J. McQueeney, and A. I. Goldman, *Phys. Rev. Lett.* **57006**, 1 (2010).

- [12] L. Luo, I. Chatzakis, A. Patz, and J. Wang, Phys. Rev. Lett. **114**, 107402 (2015); L. Luo, *et.al.*, Nat. Commun. **8**, 15565 (2014); I. Chatzakis, L. Luo, J. Wang, N.-H. Shen, T. Koschny, J. Zhou, and C. M. Soukoulis, Phys. Rev. B **86**, 125110 (2012).
- [13] A. Bardasis and J. R. Schrieffer, Phys. Rev. **121**, 1050 (1961).
- [14] A. B. Vorontsov, M. G. Vavilov, and A. V. Chubukov, Phys. Rev. B **81**, 1 (2010).
- [15] R. M. Fernandes and J. Schmalian, Phys. Rev. B **82**, (2010).
- [16] M. Beck, M. Klammer, S. Lang, P. Leiderer, V. V. Kabanov, G. N. Goltsman, and J. Demsar, Phys. Rev. Lett. **107**, 177007 (2011).
- [17] A. Rothwarf and B. N. Taylor, Phys. Rev. Lett. **19**, 27 (1967).
- [18] M. Kira and S. W. Koch. *Semiconductor Quantum Optics*. Cambridge University Press, 1st edition, (2011).
- [19] P. Nozieres and S. Schmitt-Rink, J. Low Temp. Phys. **59**, 195 (1985).
- [20] T. Papenkort, V. M. Axt, and T. Kuhn, Phys. Rev. B **76**, 1 (2007).
- [21] J. Demsar, R. D. Averitt, A. J. Taylor, V. V. Kabanov, W. N. Kang, H. J. Kim, E. M. Choi, and S. I. Lee, Phys. Rev. Lett. **91**, 267002 (2003).
- [22] A. Akbari, A. P. Schnyder, D. Manske, and I. Eremin, Europhysics Lett. **101**, 17002 (2013).
- [23] P. M. R. Brydon and C. Timm, Phys. Rev. B **80**, 1 (2009).
- [24] M. Mootz, and I. E. Perakis. *in preparation*, (2017).

APPENDIX

ROTHWARF-TAYLOR MODEL

In the conventional Rothwarf–Taylor model, the dynamics of QP and hot boson populations, $\rho(t)$ and $N(t)$ respectively, are described by coupled differential equations [17]. In the strong bottleneck regime, where the decay rate of the hot bosons is small, the pre-bottleneck dynamics can be solved analytically, yielding the QP dynamics [7]

$$\rho(t) = \frac{\beta}{R} \left[-\frac{1}{4} - \frac{1}{2\tau} + \frac{1}{\tau} \frac{1}{1 - K \exp(-t\beta/\tau)} \right]. \quad (3)$$

Here, R is the QP recombination rate while β defines the probability of pair-breaking by hot bosons. The dimensionless parameters

$$K = \frac{\frac{\tau}{2} \left(\frac{4R\rho_0}{\beta} + 1 \right) - 1}{\frac{\tau}{2} \left(\frac{4R\rho_0}{\beta} + 1 \right) + 1}, \quad \frac{1}{\tau} = \sqrt{\frac{1}{4} + \frac{2R}{\beta} (\rho_0 + 2N_0)} \quad (4)$$

are determined by the photoexcited initial QP (ρ_0) and hot boson (N_0) populations, with $-1 \leq K \leq 1$ [7]. To obtain the parameters β and R , we fit the time-delay traces of the measured THz differential reflectivity $\Delta R/R_{SC}$

shown in Fig. 3 by using Eq. (3) as in Refs. [16, 21]. However, our fits produce unphysical $K < -1$. This indicates that the conventional Rothwarf–Taylor model does not provide a consistent description of the many 100's of ps relaxation observed in FeSCs with increasing strong pump photexcitation.

MANY-BODY THEORY OF EXCITONIC SDW CORRELATION FORMATION

Hamiltonian

In this section we provide a brief overview of our microscopic theory, with full details and further calculations to be presented elsewhere [24]. We use the simplest model Hamiltonian believed to give a good qualitative description of the competition between SC and SDW order in the iron pnictides [14, 15]:

$$H = H_0 + H_\Delta + H_m. \quad (5)$$

The non-interacting part of the Hamiltonian describes the e and h Fermi sea pockets predicted by the band-structure:

$$H_0 = \sum_{\mathbf{k}, \sigma} [\xi_c(\mathbf{k}) c_{\mathbf{k}, \sigma}^\dagger c_{\mathbf{k}, \sigma} + \xi_f(\mathbf{k}) f_{\mathbf{k}, \sigma}^\dagger f_{\mathbf{k}, \sigma}]. \quad (6)$$

We include only one circular hole-like band at the Γ -point, with dispersion $\xi_c(\mathbf{k}) = \xi_{c,0} - \frac{\hbar^2 k^2}{2m_c} - \mu$, and one elliptical electron-like band with dispersion $\xi_f(\mathbf{k}) = \frac{\hbar^2 k_x^2}{2m_{fx}} + \frac{\hbar^2 k_y^2}{2m_{fy}} - \xi_{f,0} - \mu$ close to the $\mathbf{Q}_0 = (\pi, 0)/(\pi, \pi)$ pocket [14, 15]. These electron and hole energy dispersions are determined by effective masses $m_{c/f}$, energy offsets $\xi_{c/f,0}$, and chemical potential μ . The operators $f_{\mathbf{k}, \sigma}^\dagger$ ($c_{\mathbf{k}, \sigma}^\dagger$) create a carrier with crystal momentum $\hbar(\mathbf{k} - \mathbf{Q}_0)$ ($\hbar\mathbf{k}$) and spin σ in the electron-like band near \mathbf{Q}_0 (hole-like band close to the Γ -point). The SC pairing interaction [15] is given by

$$H_\Delta = V_{SC} \sum_{\mathbf{k}, \mathbf{k}'} \left[c_{\mathbf{k}, \uparrow}^\dagger c_{-\mathbf{k}, \downarrow}^\dagger f_{-\mathbf{k}', \downarrow} f_{\mathbf{k}', \uparrow} + \text{h.c.} \right], \quad (7)$$

with interaction magnitude V_{SC} . Here we only include the pair hopping between the two pockets [14, 15], which is believed to be the dominant interaction producing s^{+-} SC pairing [22]. Besides this SC interaction, the low energy properties depend on the magnetic interaction in the SDW channel [15]

$$H_m = -\frac{V_m}{2} \sum_{\mathbf{k}, \mathbf{p}, \mathbf{q}} S_z^\dagger(\mathbf{p}, \mathbf{q}) S_z(\mathbf{k}, \mathbf{q}),$$

$$S_z(\mathbf{k}, \mathbf{q}) = \sum_{\sigma} \sigma c_{\mathbf{k}, \sigma}^\dagger f_{\mathbf{k}+\mathbf{q}, \sigma}, \quad (8)$$

where V_m describes the strength of the magnetic interaction. For simplicity we neglect the coupling to phonons.

Ground-state configuration

Following previous works, the equilibrium SC properties can be described by treating the above Hamiltonian Eq.(5) in the mean-field approximation [14, 15]:

$$H_{\Delta}^{\text{MF}} = - \sum_{\mathbf{k} \in \mathcal{W}} [\Delta_c c_{-\mathbf{k}, \downarrow} c_{\mathbf{k}, \uparrow} + \Delta_f f_{-\mathbf{k}, \downarrow} f_{\mathbf{k}, \uparrow} + \text{h.c.}] , \quad (9)$$

where the SC order parameters Δ_c and Δ_f are given by [15]

$$\begin{aligned} \Delta_c &= -V_{\text{SC}} \sum_{\mathbf{p} \in \mathcal{W}} \langle f_{-\mathbf{p}, \downarrow} f_{\mathbf{p}, \uparrow} \rangle , \\ \Delta_f &= -V_{\text{SC}} \sum_{\mathbf{p} \in \mathcal{W}} \langle c_{-\mathbf{p}, \downarrow} c_{\mathbf{p}, \uparrow} \rangle . \end{aligned} \quad (10)$$

The sums in Eq.(10) only include the set \mathcal{W} of wavevectors \mathbf{k} with $|\xi_{\lambda}(\mathbf{k})| \leq \hbar\omega_C$, where ω_C is the cut-off frequency. Hartree-Fock decoupling of the magnetic interaction Eq.(8) gives [15]

$$H_{\text{m}}^{\text{MF}} = - \sum_{\mathbf{k}, \sigma} \sigma \left[M f_{\mathbf{k}+\mathbf{q}, \sigma}^{\dagger} c_{\mathbf{k}, \sigma} + M c_{\mathbf{k}, \sigma}^{\dagger} f_{\mathbf{k}+\mathbf{q}, \sigma} \right] \quad (11)$$

with SDW order parameter [15]

$$M = \frac{V_{\text{m}}}{2} \sum_{\mathbf{k}, \sigma} \sigma \langle c_{\mathbf{k}, \sigma}^{\dagger} f_{\mathbf{k}+\mathbf{q}, \sigma} \rangle \quad (12)$$

assumed to be polarized in the z -direction [23]. The SDW order is assumed for simplicity to form with a single momentum $\mathbf{Q} = \mathbf{Q}_0 + \mathbf{q}$ between the electron and hole pockets, which becomes commensurate for $\mathbf{q} = 0$. We only include this momentum in our calculations here. The mean-field Hamiltonian $H^{\text{MF}} = H_0 + H_{\text{SC}}^{\text{MF}} + H_{\text{m}}^{\text{MF}}$ is diagonalized exactly, yielding the self-consistent temperature-dependent SC and SDW gap equations that characterize the thermal equilibrium state [15]:

$$\begin{aligned} \Delta_{\lambda} &= -\frac{V_{\text{SC}}}{S} \sum_{\mathbf{k}, j} K_{\mathbf{k}, j}^{\lambda} \tanh \left(\frac{E_{j, \mathbf{k}}}{2 k_{\text{B}} T} \right) , \\ M &= \frac{V_{\text{m}}}{S} \sum_{\mathbf{k}, j} K_{\mathbf{k}, j}^{\text{m}} \tanh \left(\frac{E_{j, \mathbf{k}}}{2 k_{\text{B}} T} \right) , \end{aligned} \quad (13)$$

with kernels

$$\begin{aligned} K_{\mathbf{k}, j}^{\lambda} &= \frac{\Delta_{\bar{\lambda}} (E_{j, \mathbf{k}}^2 - \Delta_{\bar{\lambda}}^2 - \xi_{\lambda, \mathbf{k}}^2) + M^2 \Delta_{\lambda}}{2 E_{j, \mathbf{k}} (E_{j, \mathbf{k}}^2 - E_{\bar{j}, \mathbf{k}}^2)} , \\ K_{\mathbf{k}, j}^{\text{m}} &= \frac{M (E_{j, \mathbf{k}}^2 + \Delta_c \Delta_f + \xi_{c, \mathbf{k}} \xi_{f, \mathbf{k}} - M^2)}{2 E_{j, \mathbf{k}} (E_{j, \mathbf{k}}^2 - E_{\bar{j}, \mathbf{k}}^2)} , \end{aligned}$$

$$\bar{\lambda} = \begin{cases} c & \text{if } \lambda = f \\ f & \text{if } \lambda = c \end{cases}$$

$$\bar{j} = \begin{cases} 1 & \text{if } j = 2 \\ 2 & \text{if } j = 1 \end{cases}$$

and excitation energies

$$\begin{aligned} (E_{(j=1,2), \mathbf{k}})^2 &= \frac{1}{2} \left(\Gamma_{\mathbf{k}} \pm \sqrt{\Gamma_{\mathbf{k}}^2 + \Omega_{\mathbf{k}} + \tilde{\Omega}_{\mathbf{k}}} \right) , \\ \Gamma_{\mathbf{k}} &= 2 M^2 + \Delta_c^2 + \Delta_f^2 + \xi_c^2(\mathbf{k}) + \xi_f^2(\mathbf{k} + \mathbf{q}) , \\ \Omega_{\mathbf{k}} &= -4 (\xi_c^2(\mathbf{k}) + \Delta_c^2) (\xi_f^2(\mathbf{k} + \mathbf{q}) + \Delta_f^2) , \\ \tilde{\Omega}_{\mathbf{k}} &= 8 M^2 \left(\Delta_c \Delta_f + \xi_c(\mathbf{k}) \xi_f(\mathbf{k} + \mathbf{q}) - \frac{M^2}{2} \right) . \end{aligned} \quad (14)$$

To compute the equilibrium state, we solved the above mean-field gap equations self-consistently for given equilibrium chemical potential μ determined by the level x of Co doping. While the above equations may also be used to describe a quasi-thermal photoinduced state characterized by time-dependent temperature and chemical potential, the main effects of interest here come from non-thermal deviations from such quasi-thermal state, which occur prior to thermalization of the photoexcited QPs between the Fermi sea pockets.

Non-thermal dynamics

To study the photo-excited incoherent dynamics that govern our experiment, we first introduce a basis of Bogoliubov QPs, defined by the transformation

$$\begin{aligned} c_{\mathbf{k}, \uparrow} &= u_{\mathbf{k}} \alpha_{\mathbf{k}}^{\dagger} - v_{\mathbf{k}} \beta_{\mathbf{k}} + \bar{u}_{\mathbf{k}} \gamma_{\mathbf{k}}^{\dagger} + \bar{v}_{\mathbf{k}} \delta_{\mathbf{k}} , \\ c_{-\mathbf{k}, \downarrow}^{\dagger} &= v_{\mathbf{k}} \alpha_{\mathbf{k}}^{\dagger} + u_{\mathbf{k}} \beta_{\mathbf{k}} + \bar{v}_{\mathbf{k}} \gamma_{\mathbf{k}}^{\dagger} - \bar{u}_{\mathbf{k}} \delta_{\mathbf{k}} , \\ f_{\mathbf{k}+\mathbf{q}, \uparrow} &= w_{\mathbf{k}} \alpha_{\mathbf{k}}^{\dagger} + x_{\mathbf{k}} \beta_{\mathbf{k}} + \bar{w}_{\mathbf{k}} \gamma_{\mathbf{k}}^{\dagger} - \bar{x}_{\mathbf{k}} \delta_{\mathbf{k}} , \\ f_{-\mathbf{k}-\mathbf{q}, \downarrow}^{\dagger} &= x_{\mathbf{k}} \alpha_{\mathbf{k}}^{\dagger} - w_{\mathbf{k}} \beta_{\mathbf{k}} + \bar{x}_{\mathbf{k}} \gamma_{\mathbf{k}}^{\dagger} + \bar{w}_{\mathbf{k}} \delta_{\mathbf{k}} . \end{aligned} \quad (15)$$

Here, $u_{\mathbf{k}}$, $v_{\mathbf{k}}$, $w_{\mathbf{k}}$, $x_{\mathbf{k}}$, $\bar{u}_{\mathbf{k}}$, $\bar{v}_{\mathbf{k}}$, $\bar{w}_{\mathbf{k}}$, and $\bar{x}_{\mathbf{k}}$ are coherence factors that depend on the instantaneous SC and SDW order parameters. We include for simplicity only a single momentum \mathbf{q} in H_{Δ} and H_{m} as discussed above. Since we are interested in SDW excitonic state formation, we consider the full inter-pocket SDW interaction Eq. (8) without factorization, which introduces relaxation driven by the inter-band interaction. On the other hand, the SC interaction is treated within the mean-field approximation for simplicity.

Substituting Eq.(15) into the above Hamiltonian and eliminating the off-diagonal quadratic contributions, we transform the Hamiltonian in the QP basis for given order parameters Δ_c , Δ_f and M :

$$\begin{aligned} H_{\text{BCS}} &= H_0 + H_{\Delta}^{\text{MF}} \\ &= \sum_{\mathbf{k}} \left[R_{\mathbf{k}}^{-} \left(\alpha_{\mathbf{k}}^{\dagger} \alpha_{\mathbf{k}} + \beta_{\mathbf{k}}^{\dagger} \beta_{\mathbf{k}} \right) + R_{\mathbf{k}}^{+} \left(\gamma_{\mathbf{k}}^{\dagger} \gamma_{\mathbf{k}} + \delta_{\mathbf{k}}^{\dagger} \delta_{\mathbf{k}} \right) \right] , \end{aligned} \quad (16)$$

where we introduced

$$\begin{aligned} R_{\mathbf{k}}^- &= \xi_c(\mathbf{k}) (v_{\mathbf{k}}^2 - u_{\mathbf{k}}^2) + \xi_f(\mathbf{k} + \mathbf{q}) (x_{\mathbf{k}}^2 - w_{\mathbf{k}}^2) \\ &\quad - 2(u_{\mathbf{k}}v_{\mathbf{k}}\Delta_c + x_{\mathbf{k}}w_{\mathbf{k}}\Delta_f), \\ R_{\mathbf{k}}^+ &= \xi_c(\mathbf{k}) (\bar{v}_{\mathbf{k}}^2 - \bar{u}_{\mathbf{k}}^2) + \xi_f(\mathbf{k} + \mathbf{q}) (\bar{x}_{\mathbf{k}}^2 - \bar{w}_{\mathbf{k}}^2) \\ &\quad - 2(\bar{u}_{\mathbf{k}}\bar{v}_{\mathbf{k}}\Delta_c + \bar{x}_{\mathbf{k}}\bar{w}_{\mathbf{k}}\Delta_f). \end{aligned} \quad (17)$$

and

$$\begin{aligned} H_m &= -\frac{V_m}{2} \sum_{\mathbf{k}, \mathbf{p}} [2l_{\mathbf{k}}m_{\mathbf{p}} (\alpha_{\mathbf{p}}^\dagger\alpha_{\mathbf{p}} + \beta_{\mathbf{p}}^\dagger\beta_{\mathbf{p}}) \\ &\quad + 2l_{\mathbf{k}}p_{\mathbf{p}} (\gamma_{\mathbf{p}}^\dagger\gamma_{\mathbf{p}} + \delta_{\mathbf{p}}^\dagger\delta_{\mathbf{p}}) \\ &\quad + m_{\mathbf{k}}m_{\mathbf{p}} (\alpha_{\mathbf{p}}^\dagger\alpha_{\mathbf{p}} + \beta_{\mathbf{p}}^\dagger\beta_{\mathbf{p}}) (\alpha_{\mathbf{k}}^\dagger\alpha_{\mathbf{k}} + \beta_{\mathbf{k}}^\dagger\beta_{\mathbf{k}}) \\ &\quad + p_{\mathbf{k}}p_{\mathbf{p}} (\gamma_{\mathbf{p}}^\dagger\gamma_{\mathbf{p}} + \delta_{\mathbf{p}}^\dagger\delta_{\mathbf{p}}) (\gamma_{\mathbf{k}}^\dagger\gamma_{\mathbf{k}} + \delta_{\mathbf{k}}^\dagger\delta_{\mathbf{k}}) \\ &\quad + p_{\mathbf{k}}m_{\mathbf{p}} (\alpha_{\mathbf{p}}^\dagger\alpha_{\mathbf{p}} + \beta_{\mathbf{p}}^\dagger\beta_{\mathbf{p}}) (\gamma_{\mathbf{k}}^\dagger\gamma_{\mathbf{k}} + \delta_{\mathbf{k}}^\dagger\delta_{\mathbf{k}}) \\ &\quad + (r_{\mathbf{k}}r_{\mathbf{p}} + s_{\mathbf{k}}s_{\mathbf{p}}) \tilde{S}_z^\dagger(\mathbf{p})\tilde{S}(\mathbf{k}) \\ &\quad + (\bar{r}_{\mathbf{k}}\bar{r}_{\mathbf{p}} + \bar{s}_{\mathbf{k}}\bar{s}_{\mathbf{p}}) \bar{S}_z^\dagger(\mathbf{p})\bar{S}(\mathbf{k})] \end{aligned} \quad (18)$$

with coherence factors

$$\begin{aligned} l_{\mathbf{k}} &= 2(u_{\mathbf{k}}w_{\mathbf{k}} + \bar{u}_{\mathbf{k}}\bar{w}_{\mathbf{k}}), \quad m_{\mathbf{k}} = (u_{\mathbf{k}}w_{\mathbf{k}} + v_{\mathbf{k}}x_{\mathbf{k}}), \\ p_{\mathbf{k}} &= (\bar{u}_{\mathbf{k}}\bar{w}_{\mathbf{k}} + \bar{v}_{\mathbf{k}}\bar{x}_{\mathbf{k}}), \quad r_{\mathbf{k}} = v_{\mathbf{k}}\bar{w}_{\mathbf{k}} + \bar{v}_{\mathbf{k}}w_{\mathbf{k}}, \\ s_{\mathbf{k}} &= (\bar{u}_{\mathbf{k}}x_{\mathbf{k}} + \bar{x}_{\mathbf{k}}u_{\mathbf{k}}), \quad \bar{r}_{\mathbf{k}} = \bar{v}_{\mathbf{k}}x_{\mathbf{k}} + u_{\mathbf{k}}\bar{w}_{\mathbf{k}}, \\ \bar{s}_{\mathbf{k}} &= v_{\mathbf{k}}\bar{x}_{\mathbf{k}} + \bar{u}_{\mathbf{k}}w_{\mathbf{k}}. \end{aligned} \quad (19)$$

The last two lines in Equation (18) describe the deviations from the mean field Hamiltonian and involve four QP operators (two pairs of QPs). The collective effects in the SDW channel are described by the QP pair operators

$$\tilde{S}_z(\mathbf{k}) = \beta_{\mathbf{k}}\gamma_{\mathbf{k}} + \alpha_{\mathbf{k}}\delta_{\mathbf{k}}, \quad \bar{S}_z(\mathbf{k}) = \beta_{\mathbf{k}}^\dagger\delta_{\mathbf{k}} - \alpha_{\mathbf{k}}^\dagger\gamma_{\mathbf{k}}. \quad (20)$$

Since we are interested in long timescales after dephasing of any coherences among QPs, we only keep the QP number-conserving terms in Eqs. (16) and (18) and neglect any photoinduced coherence among QPs, $\langle \tilde{S}_z(\mathbf{k}) \rangle = \langle \bar{S}_z(\mathbf{k}) \rangle = 0$. The transformation of the SC and SDW gap equations in the QP basis then yields

$$\begin{aligned} \Delta_c &= -V_{SC} \sum_{\mathbf{k}} \left[u_{\mathbf{k}}v_{\mathbf{k}} (1 - n_{\mathbf{k}}^\alpha - n_{\mathbf{k}}^\beta) \right. \\ &\quad \left. + \bar{u}_{\mathbf{k}}\bar{v}_{\mathbf{k}} (1 - n_{\mathbf{k}}^\gamma - n_{\mathbf{k}}^\delta) \right], \\ \Delta_f &= -V_{SC} \sum_{\mathbf{k}} \left[w_{\mathbf{k}}x_{\mathbf{k}} (1 - n_{\mathbf{k}}^\alpha - n_{\mathbf{k}}^\beta) \right. \\ &\quad \left. + \bar{w}_{\mathbf{k}}\bar{x}_{\mathbf{k}} (1 - n_{\mathbf{k}}^\gamma - n_{\mathbf{k}}^\delta) \right], \\ M &= -\frac{V_m}{2} \sum_{\mathbf{k}} \left[2l_{\mathbf{k}} - m_{\mathbf{k}} (n_{\mathbf{k}}^\alpha + n_{\mathbf{k}}^\beta) - p_{\mathbf{k}} (n_{\mathbf{k}}^\gamma + n_{\mathbf{k}}^\delta) \right], \end{aligned} \quad (21)$$

where we introduced the QP distributions

$$\begin{aligned} n_{\mathbf{k}}^\alpha &= \langle \alpha_{\mathbf{k}}^\dagger\alpha_{\mathbf{k}} \rangle, \quad n_{\mathbf{k}}^\beta = \langle \beta_{\mathbf{k}}^\dagger\beta_{\mathbf{k}} \rangle, \quad n_{\mathbf{k}}^\gamma = \langle \gamma_{\mathbf{k}}^\dagger\gamma_{\mathbf{k}} \rangle, \\ n_{\mathbf{k}}^\delta &= \langle \delta_{\mathbf{k}}^\dagger\delta_{\mathbf{k}} \rangle. \end{aligned} \quad (22)$$

As in the simple BCS theory, the excitation of QP populations quenches both the SC and the SDW order parameters. We simplify the problem by assuming that, after the initial sub-ps QP relaxation, the QP distributions are all similar for high frequency optical pump excitation at $\sim 1.5\text{eV}$: $n_{\mathbf{k}}^\alpha \approx n_{\mathbf{k}}^\beta \equiv n_{\mathbf{k}}^{\alpha\beta}$ and $n_{\mathbf{k}}^\gamma \approx n_{\mathbf{k}}^\delta \equiv n_{\mathbf{k}}^{\gamma\delta}$. The time evolution of the SC and SDW order parameters monitored by the THz probe is determined by the time evolution of the above QP populations, which we describe by deriving equations of motion using the full above Hamiltonian. The scattering processes determined by H_m lead to QP relaxation described by

$$\begin{aligned} \frac{\partial}{\partial t} n_{\mathbf{p}}^{\alpha\beta} &= \frac{V_m}{\hbar} \text{Im} \sum_{\mathbf{k}} \left[(r_{\mathbf{k}}r_{\mathbf{p}} + s_{\mathbf{k}}s_{\mathbf{p}}) C_{SDW,1}^{\mathbf{k},\mathbf{p}} \right. \\ &\quad \left. + (\bar{r}_{\mathbf{k}}\bar{r}_{\mathbf{p}} + \bar{s}_{\mathbf{k}}\bar{s}_{\mathbf{p}}) C_{SDW,2}^{\mathbf{k},\mathbf{p}} \right], \\ \frac{\partial}{\partial t} n_{\mathbf{p}}^{\gamma\delta} &= \frac{V_m}{\hbar} \text{Im} \sum_{\mathbf{k}} \left[(r_{\mathbf{k}}r_{\mathbf{p}} + s_{\mathbf{k}}s_{\mathbf{p}}) C_{SDW,1}^{\mathbf{k},\mathbf{p}} \right. \\ &\quad \left. - (\bar{r}_{\mathbf{k}}\bar{r}_{\mathbf{p}} + \bar{s}_{\mathbf{k}}\bar{s}_{\mathbf{p}}) C_{SDW,2}^{\mathbf{k},\mathbf{p}} \right]. \end{aligned} \quad (23)$$

The higher density matrices C_{SDW} that appear on the right-hand side of the above equations involve four QP operators and are defined after subtracting all factorizable contributions by using a cluster-expansion as in [18]:

$$C_{SDW,1}^{\mathbf{p},\mathbf{k}} = \Delta \langle \tilde{S}_z^\dagger(\mathbf{k})\tilde{S}_z(\mathbf{p}) \rangle, \quad C_{SDW,2}^{\mathbf{p},\mathbf{k}} = \Delta \langle \bar{S}_z^\dagger(\mathbf{k})\bar{S}_z(\mathbf{p}) \rangle. \quad (24)$$

For $C_{SDW}=0$ we recover the mean-field results, while the four-QP density matrices describe correlation build-up and scattering among QPs. Such processes modify the QP distributions as compared to mean field, which leads to time-dependent SC order parameter quench. The equations of motion of C_{SDW} describe the time evolution of correlations among the photoexcited QPs and are derived similar to Ref. [18]:

$$\begin{aligned} i\hbar \frac{\partial}{\partial t} C_{SDW,1}^{\mathbf{p},\mathbf{k}} &= (\varepsilon_{\mathbf{p}}^- + \varepsilon_{\mathbf{p}}^+ - \varepsilon_{\mathbf{k}}^- - \varepsilon_{\mathbf{k}}^+) C_{SDW,1}^{\mathbf{p},\mathbf{k}} + S_1^{\mathbf{p},\mathbf{k}} \\ &\quad + 2V_m (1 - n_{\mathbf{k}}^{\alpha\beta} - n_{\mathbf{k}}^{\gamma\delta}) \sum_{\mathbf{l}} (r_{\mathbf{k}}r_{\mathbf{l}} + s_{\mathbf{k}}s_{\mathbf{l}}) C_{SDW,1}^{\mathbf{p},\mathbf{l}} \\ &\quad - 2V_m (1 - n_{\mathbf{k}}^{\alpha\beta} - n_{\mathbf{k}}^{\gamma\delta}) \sum_{\mathbf{l}} (r_{\mathbf{p}}r_{\mathbf{l}} + s_{\mathbf{p}}s_{\mathbf{l}}) C_{SDW,1}^{\mathbf{l},\mathbf{k}} \\ &\quad + D_1^{\mathbf{p},\mathbf{k}} + T_1^{\mathbf{p},\mathbf{k}}, \end{aligned} \quad (25)$$

$$\begin{aligned} i\hbar \frac{\partial}{\partial t} C_{SDW,2}^{\mathbf{p},\mathbf{k}} &= (\varepsilon_{\mathbf{p}}^- - \varepsilon_{\mathbf{p}}^+ - \varepsilon_{\mathbf{k}}^- + \varepsilon_{\mathbf{k}}^+) C_{SDW,2}^{\mathbf{p},\mathbf{k}} + S_2^{\mathbf{p},\mathbf{k}} \\ &\quad + 2V_m (n_{\mathbf{k}}^{\alpha\beta} - n_{\mathbf{k}}^{\gamma\delta}) \sum_{\mathbf{l}} (\bar{r}_{\mathbf{k}}\bar{r}_{\mathbf{l}} + \bar{s}_{\mathbf{k}}\bar{s}_{\mathbf{l}}) C_{SDW,2}^{\mathbf{p},\mathbf{l}} \\ &\quad - 2V_m (n_{\mathbf{k}}^{\alpha\beta} - n_{\mathbf{k}}^{\gamma\delta}) \sum_{\mathbf{l}} (\bar{r}_{\mathbf{p}}\bar{r}_{\mathbf{l}} + \bar{s}_{\mathbf{p}}\bar{s}_{\mathbf{l}}) C_{SDW,2}^{\mathbf{l},\mathbf{k}} \\ &\quad + D_2^{\mathbf{p},\mathbf{k}} + T_2^{\mathbf{p},\mathbf{k}}, \end{aligned} \quad (26)$$

where the QP energies are given by

$$\begin{aligned}\varepsilon_{\mathbf{k}}^- &= \xi_c(\mathbf{k}) (v_{\mathbf{k}}^2 - u_{\mathbf{k}}^2) + \xi_f(\mathbf{k} + \mathbf{q}) (x_{\mathbf{k}}^2 - w_{\mathbf{k}}^2) \\ &\quad - 2(u_{\mathbf{k}}v_{\mathbf{k}}\Delta_c + x_{\mathbf{k}}w_{\mathbf{k}}\Delta_f) - 2(u_{\mathbf{k}}w_{\mathbf{k}} + v_{\mathbf{k}}x_{\mathbf{k}})M, \\ \varepsilon_{\mathbf{k}}^+ &= \xi_c(\mathbf{k}) (\bar{v}_{\mathbf{k}}^2 - \bar{u}_{\mathbf{k}}^2) + \xi_f(\mathbf{k} + \mathbf{q}) (\bar{x}_{\mathbf{k}}^2 - \bar{w}_{\mathbf{k}}^2) \\ &\quad - 2(\bar{u}_{\mathbf{k}}\bar{v}_{\mathbf{k}}\Delta_c + \bar{x}_{\mathbf{k}}\bar{w}_{\mathbf{k}}\Delta_f) - 2(\bar{u}_{\mathbf{k}}\bar{w}_{\mathbf{k}} + \bar{v}_{\mathbf{k}}\bar{x}_{\mathbf{k}})M. \quad (27)\end{aligned}$$

The usual scattering among individual QPs is described by the source terms

$$\begin{aligned}S_1^{\mathbf{p},\mathbf{k}} &= \frac{4V_m}{S} (r_{\mathbf{k}}r_{\mathbf{p}} + s_{\mathbf{k}}s_{\mathbf{p}}) \left[n_{\mathbf{p}}^{\alpha\beta} n_{\mathbf{p}}^{\gamma\delta} (1 - n_{\mathbf{k}}^{\alpha\beta})(1 - n_{\mathbf{k}}^{\gamma\delta}) \right. \\ &\quad \left. - n_{\mathbf{k}}^{\alpha\beta} n_{\mathbf{k}}^{\gamma\delta} (1 - n_{\mathbf{p}}^{\alpha\beta})(1 - n_{\mathbf{p}}^{\gamma\delta}) \right], \quad (28)\end{aligned}$$

$$\begin{aligned}S_2^{\mathbf{p},\mathbf{k}} &= \frac{4V_m}{S} (\bar{r}_{\mathbf{k}}\bar{r}_{\mathbf{p}} + \bar{s}_{\mathbf{k}}\bar{s}_{\mathbf{p}}) \left[n_{\mathbf{k}}^{\alpha\beta} n_{\mathbf{p}}^{\gamma\delta} (1 - n_{\mathbf{p}}^{\alpha\beta})(1 - n_{\mathbf{k}}^{\gamma\delta}) \right. \\ &\quad \left. - n_{\mathbf{k}}^{\alpha\beta} n_{\mathbf{p}}^{\gamma\delta} (1 - n_{\mathbf{p}}^{\alpha\beta})(1 - n_{\mathbf{k}}^{\gamma\delta}) \right]. \quad (29)\end{aligned}$$

$S_{1,2}^{\mathbf{p},\mathbf{k}}$ have the typical form describing Boltzmann scattering with in- and out-scattering contributions. The first line in Eqs. (25) and (26) describe relaxation among individual quasi-particles within the Born approximation, without any excitonic correlation. Such perturbative Born scattering approximation does not change the behavior at long 100's ps times.

The next two lines on the rhs of Eqs. (25) and (26) give the most important contributions here. As soon as non-thermal QP populations are excited in the e and h Fermi sea pockets, $S^{\mathbf{p},\mathbf{k}} \neq 0$ and the above equations describe screening build-up and formation of spin-excitons among the laser-induced QPs. Renormalization of the QP energies and screening-type effects are described by the remaining two-particle contributions $D_{1,2}^{\mathbf{p},\mathbf{k}}$. The coupling to three-particle correlations, $T_{1,2}^{\mathbf{p},\mathbf{k}}$, introduces relaxation of the SDW excitonic correlation.

$C_{\text{SDW},2}^{\mathbf{p},\mathbf{k}}$ is mostly significant in the strong excitation regime, as it requires an appreciable imbalance between QP distributions such that $(n_{\mathbf{k}}^{\alpha\beta} - n_{\mathbf{k}}^{\gamma\delta})$ is non-vanishing. In contrast, $C_{\text{SDW},1}^{\mathbf{p},\mathbf{k}}$ becomes large already at low QP densities. Here we assume that high-frequency pump excitation results in similar nonthermal densities of α -, β - and γ -, δ - QPs, so we neglect $C_{\text{SDW},2}^{\mathbf{p},\mathbf{k}}$. More details on the full theory will be presented elsewhere [24].

Generalized Wannier equation for describing the excitonic correlation

Following an initial temporal regime of ultrafast SC gap quenching, the QP distributions $n_{\mathbf{k}}^{\alpha\beta}$ and $n_{\mathbf{k}}^{\gamma\delta}$ change adiabatically with time, so we seek stationary solutions of Eq. (25). The form of these equations of motion suggests the transformation of the SDW correlation $C_{\text{SDW},1}^{\mathbf{p},\mathbf{k}}$ into

an excitonic basis [18] defined by the wavefunction $\phi_{\nu,\mathbf{q}}^r$. The latter is given by the generalized Wannier equation

$$\begin{aligned}(\varepsilon_{\mathbf{p}}^- + \varepsilon_{\mathbf{p}}^+) \phi_{\nu}^r(\mathbf{p}) - (1 - n_{\mathbf{p}}^{\alpha\beta} - n_{\mathbf{p}}^{\gamma\delta}) \sum_{\mathbf{k}} V_{\mathbf{k},\mathbf{p}} \phi_{\nu}^r(\mathbf{k}) \\ = E_{\nu} \phi_{\nu}^r(\mathbf{p}), \quad (30)\end{aligned}$$

where the Coulomb matrix element depends on the QP coherence factors:

$$\begin{aligned}V_{\mathbf{k},\mathbf{p}} &= 2V_m [(\bar{u}_{\mathbf{k}}x_{\mathbf{k}} + \bar{x}_{\mathbf{k}}u_{\mathbf{k}})(\bar{u}_{\mathbf{p}}x_{\mathbf{p}} + \bar{x}_{\mathbf{p}}u_{\mathbf{p}}) \\ &\quad + (v_{\mathbf{k}}\bar{w}_{\mathbf{k}} + \bar{v}_{\mathbf{k}}w_{\mathbf{k}})(v_{\mathbf{p}}\bar{w}_{\mathbf{p}} + \bar{v}_{\mathbf{p}}w_{\mathbf{p}})]. \quad (31)\end{aligned}$$

It is then convenient to introduce the excitonic operator

$$X_{\nu} = \sum_{\mathbf{p}} \phi_{\nu}^{1*}(\mathbf{p}) \tilde{S}_z(\mathbf{p}). \quad (32)$$

Unlike for phonons, the commutation relations of this composite exciton operator have non-bosonic corrections due to Phase Space Filling arising from the fermionic character of the QPs involved. By transforming from uncorrelated QPs to the excitonic basis

$$\tilde{S}_z(\mathbf{p}) = \sum_{\nu} \phi_{\nu}^r(\mathbf{p}) X_{\nu} \quad (33)$$

we describe the correlations of interest in terms of the above-defined spin-excitons:

$$\begin{aligned}C_{\text{SDW},1}^{\mathbf{p},\mathbf{k}} &= \sum_{\nu,\nu'} [\phi_{\nu}^r(\mathbf{k})]^* \phi_{\nu'}^r(\mathbf{p}) \Delta \langle X_{\nu}^{\dagger} X_{\nu'} \rangle, \\ \Delta \langle X_{\nu}^{\dagger} X_{\nu'} \rangle &= \sum_{\mathbf{k},\mathbf{p}} \phi_{\nu}^l(\mathbf{k}) [\phi_{\nu'}^l(\mathbf{p})]^* C_{\text{SDW},1}^{\mathbf{p},\mathbf{k}}. \quad (34)\end{aligned}$$

The coupling of the QP distributions to the excitonic amplitude in Eq. (30) yields a non-hermitian eigenvalue problem, so we obtain left- and right-handed eigenfunctions $\phi_{\nu,\mathbf{q}}^{r,l}$. These describe both bound and scattering solutions, where the latter correspond to unbound QP pairs whose properties are modified by the magnetic interaction. The above wavefunctions satisfy the orthogonality and completeness relations

$$\sum_{\mathbf{p}} [\phi_{\nu}^l(\mathbf{p})]^* \phi_{\nu'}^r(\mathbf{p}) = \delta_{\nu,\nu'}, \quad \sum_{\nu} [\phi_{\nu}^l(\mathbf{p})]^* \phi_{\nu'}^r(\mathbf{p}') = \delta_{\mathbf{p},\mathbf{p}'}. \quad (35)$$

To simplify the problem for our purposes here, we assume relaxation to the lowest spin-exciton state $\phi_{\mathbf{p}} \equiv \phi_{\nu=0}^r(\mathbf{p})$ and only retain this contribution to Eq. (34). As a result,

$$C_{\text{SDW},1}^{\mathbf{p},\mathbf{k}} = \phi_{\mathbf{p}}^* \phi_{\mathbf{k}}, \quad (36)$$

where we have absorbed $\Delta \langle X_{\nu=0}^{\dagger} X_{\nu=0} \rangle$ into $\phi_{\mathbf{p}}$.

In the incoherent long-time regime and for $C_{\text{SDW},1}^{\mathbf{p},\mathbf{k}}$ dominating over $C_{\text{SDW},2}^{\mathbf{p},\mathbf{k}}$, we obtain Eq. (2) from an exact relation between the traces of the corresponding density

matrices. [24]. The coupled Eqs. (2) and (30), together with the order parameter equations (21) and coherent factor expressions, yield a self-consistent calculation of the many-body state defined by $(\phi_{\mathbf{p}}, n_{\mathbf{p}}, \Delta_c, \Delta_f, M)$. This result corresponds to an adiabatic solution of the equations of motion and describes the non-equilibrium state reached after formation/buildup of SDW correlation and before the system thermalizes via scattering across the Fermi sea pockets.

Numerical Calculations

In our numerical calculations presented in Fig. 4, we first computed the thermal ground state configuration by solving the SDW and SC gap equations (13) self-consistently for a given doping level. We then solved Eqs. (1) and (2) together with the order parameter equations iteratively until convergence was reached. The energy eigenvalue E determines the total QP density $\rho = 1/S \sum_{\mathbf{k}} n_{\mathbf{k}}$ and thus corresponds to excitonic corrections to the chemical potential. In all numerical calculations we used typical parameters of $\text{Ba}(\text{Fe}_{1-x}\text{Co}_x)_2\text{As}_2$, which yield a good qualitative agreement with the experimentally observed doping dependence of the SC and

SDW orders [15]. To model the photoinduced initial condition immediately after the initial phonon-induced ultrafast SC gap quench following photocarrier relaxation, we assume that the excited QPs have relaxed into the different pockets and describe their distributions for simplicity by Fermi-Dirac distributions

$$\begin{aligned} n_{\mathbf{k}}^{\alpha,\beta} &= \frac{1}{1 + \exp(\varepsilon_{\mathbf{k}}^-/k_B T_{\alpha,\beta})}, \\ n_{\mathbf{k}}^{\gamma,\delta} &= \frac{1}{1 + \exp(\varepsilon_{\mathbf{k}}^+/k_B T_{\gamma,\delta})} \end{aligned} \quad (37)$$

which determine the initial condition to our time-dependent calculation. The temperatures $T_{\alpha,\beta}$ and $T_{\gamma,\delta}$ are obtained from the total QP densities

$$\rho_{\alpha,\beta} = \frac{1}{S} \sum_{\mathbf{k}} n_{\mathbf{k}}^{\alpha,\beta}, \quad \rho_{\gamma,\delta} = \frac{1}{S} \sum_{\mathbf{k}} n_{\mathbf{k}}^{\gamma,\delta}. \quad (38)$$

In the actual calculations presented here, $T_{\alpha,\beta}$ and $T_{\gamma,\delta}$ were chosen such that the total densities of the different QPs are the same, i. e. $\rho \equiv \rho_{\alpha,\beta} = \rho_{\gamma,\delta}$. However, our conclusions do not depend on how we describe the initial QP distributions, which form following relaxation of the photocarriers from high energy states populated by the pump that are not well known.